Snow Avalanches

Christophe Ancey

Cemagref, unité Erosion Torrentielle, Neige et Avalanches, Domaine Universitaire, 38402 Saint-Martin-d'Hères Cedex, France

1   Introduction

Over the last century, mountain ranges in Europe and North America have seen substantial development due to the increase in recreational activities, transportation, construction in high altitude areas, etc. In these mountain ranges, avalanches often threaten man's activities and life. Typical examples include recent disasters, such as the avalanche at Val d'Isère in 1970 (39 people were killed in a hostel) or the series of catastrophic avalanches throughout the Northern Alps in February 1999 (62 residents killed). The rising demand for higher safety measures has given new impetus to the development of mitigation technology and has given rise to a new scientific area entirely devoted to snow and avalanches. This paper summarises the paramount features of avalanches (formation and motion) and outlines the main approaches used for describing their movement. We do not tackle specific problems related to snow mechanics and avalanche forecasting. For more information on the subject, the reader is referred to the main textbooks published in Alpine countries [1–8].

1.1   A physical picture of avalanches

Avalanches are rapid gravity-driven masses of snow moving down mountain slopes. With this fairly long definition, we try to characterise avalanches with respect to other snow flows. For instance, a snowdrift involves transport of snow particles, driven not by gravity but by wind. The slow slide and creep of the snow cover is driven by gravity but with a slow kinetic (typical velocities are in mm/day). Likewise, the slide of a snowpack down a roof cannot be considered to be an avalanche.

1.2   Avalanche release

Successive snowfalls during the winter and spring accumulate to form snow cover. Depending on the weather conditions, significant changes in snow (types of crystal) occur as a result of various mechanical (creep, settlement) and thermo-dynamic processes (mass transfer). This induces considerable variations in its mechanical properties (cohesion, shear strength). Due to its layer structure, the snow cover is liable to internal slides between layers induced by gravity. When the shear deformation exceeds the maximum value that the layers of snow can

undergo, a failure arises, usually developing first along the sliding surface, then propagating throughout the upper layers across a crack perpendicular to the downward direction. This kind of release is very frequent. In the field evidence of such failures consists of a clear fracture corresponding to the breakaway wall at the top edge of the slab and a bed surface over which the slab has slid (see Fig. 1). If the snow is too loose, the failure processes differ significantly from the ones governing slab release. Loose snow avalanches form near the surface. They usually start from a single point, then they spread out laterally by pushing and incorporating more snow.

Fig. 1. Slab avalanche released by gliding wet snow

The stability of a snow cover depends on many parameters. We can distinguish the fixed parameters related to the avalanche path and the varying parameters, generally connected to weather conditions. Fixed parameters include:

- *Mean slope*. In most cases, the average inclination of starting zones ranges from 27° to 50° On rare occasions, avalanches can start on gentle slopes of less than 25° (e.g. *slushflow* involving wet snow with high water content), but generally the shear stress induced by gravity is not large enough to cause failure. For inclinations in excess of 45° to 50°, many slides (*sluffs*) occur during snowfalls; thus amounts of snow deposited on steep slopes are limited.
- *Roughness*. Ground surface roughness is a key factor in the anchorage of the snow cover to the ground. Dense forests, broken terrain, starting zones cut by several ridges, ground covered by large boulders generally limit the amount of snow that can be involved in the start of an avalanche. Conversely, widely-spaced forests, large and open slopes with smooth ground may favour avalanche release.

- *Shape and curvature of starting zone.* The stress distribution within the snowpack and the variation in its depth depend on the longitudinal shape of the ground. For instance, convex slopes concentrate tensile stresses and are generally associated with a significant variation in the snowcover depth, favouring snowpack instability.
- *Orientation to the sun.* The orientation of slopes with respect to the sun has a strong influence on the day-to-day stability of the snowpack. For instance, in winter, shady slopes receive little incoming radiation from the sun and conversely lose heat by long-wave radiation. It is generally observed that for these slopes, the snowpack is cold and tends to develop weak layers (faceted crystals, depth hoar). Many fatalities occur each year in such conditions. In late winter and in spring, the temperature increase enhances stability of snowpacks on shady slopes and instability on sunny slopes.

Among the varying factors intervening in avalanche release, experience clearly shows that in most cases, avalanches result from changes in weather conditions:

- *New snow.* Most of the time, snowfall is the cause of avalanches. The hazard increases significantly with the increase in the depth of new snow. For instance, an accumulation of 30 cm/day may be sufficient to cause widespread avalanching. In European mountain ranges, heavy snowfalls with a total precipitation exceeding 1 m during the previous three days may produce large avalanches, with possible extension down to the valley bottom.
- *Wind.* The wind is an additional factor which significantly influences the stability of a snowpack. Indeed it causes uneven snow redistribution (accumulation on lee slopes), accelerates snow metamorphism, forms cornices, whose collapses may trigger avalanches. On the whole, influence of the wind is very diverse, either consolidating snow (compacting and rounding snow crystals) or weakening it.
- *Rain and liquid water content.* The rain plays a complex role in snow metamorphism. Generally, for dry snow, a small increase in the liquid water content (LWC<0.5%) does not significantly affect the mechanical properties of snow. However, heavy rain induces a rapid and noticeable increase in LWC, which results in a drop in the shear stress strength. This situation leads to widespread avalanche activity (wet snow avalanches).
- *Snowpack structure.* A given snowpack results from the successive snowfalls. The stability of the resulting layer structure depends a great deal on the bonds between layers and their cohesion. For instance, heterogeneous snowpacks, made up of weak and stiff layers, are more unstable than homogenous snowpacks.

1.3   Avalanche motion

It is very common and helpful to consider two limiting cases of avalanches depending on the form of motion [7]:

- The *flowing avalanche* (avalanche coulante, Fliesslawine, valanga radente): a flowing avalanche is an avalanche with a high-density core at the bottom. Motion is dictated by the relief. The flow depth does not generally exceed a few meters (see Fig. 2). The typical mean velocity ranges from 5 m/s to 25 m/s. On average, the density is fairly high, generally ranging from 150 kg/m^3 to 500 kg/m^3.
- The *airborne avalanche* (avalanche en aérosol, Staublawine, valanga nubiforme): it is a very rapid flow of a snow cloud, in which most of the snow particles are suspended in the ambient air by turbulence (see Fig. 3). Relief has usually little influence on this aerial flow. Typically, for the flow depth, mean velocity, and mean density, the order of magnitude is 10–100 m, 50–100 m/s, 5–50 kg/m^3 respectively.

Fig. 2. Flowing avalanche impacting a wing-shaped structure in the Lauratet experimental site (France)

The avalanche classification proposed here only considers the form of motion and not the quality of snow. In the literature, other terms and classifications have been used. For instance, it is very frequent to see terms such as dry-snow avalanches, wet-snow avalanches, powder avalanches, etc. In many cases and probably in most cases in ordinary conditions, the motion form is directly influenced by the quality of snow in the starting zone. For instance, on a sufficiently steep slope, dry powder snow often gives rise to an airborne avalanche (in this case no confusion is possible between airborne and powder snow avalanches). However, in some cases, especially for extreme avalanches (generally involving large volumes of snow), motion is independent of the snow type. For instance, wet snow may be associated with airborne (e.g., Favrand avalanche in the Cha-

Fig. 3. Airborne avalanche descending a steep slope (Himalayas)

monix valley, France, on 16 May 1983). Between the two limiting cases above, there is a fairly wide variety of avalanches, which exhibit characteristics common to both airborne and flowing avalanches. Sometimes, such flows are referred to as "mixed-motion avalanches". The use of this term is often inappropriate because it should be restricted to describing complex flows for which both the dense core and the airborne play a role (from a dynamic point of view). In some cases, the dense core is covered with a snow dust cloud, made up of snow particles suspended by turbulent eddies of air resulting from the friction exerted by the air on the core. This cloud can entirely hide the high-density core, giving the appearance of an airborne avalanche, but in fact, it plays no significant role in avalanche dynamics. It should be born in mind that the mere observation of a cloud is generally not sufficient to specify the type of an avalanche. Further elements such as the features of the deposit or the destructive effects are required.

The current terminology asserts that there are two main types of motion. In this respect, mixed-motion avalanches are seen as avalanches combining aspects of both airborne and flowing avalanches, but they are not seen as a third type of avalanche. The question of a third type of avalanche has been raised by some experts during the last few years. Indeed, there is field evidence that some events did not belong either to the group of airborne or flowing avalanches. For instance, the Taconnaz avalanche (Haute-Savoie, France) on 11 February 1999 severely damaged two concrete-reinforced structures. The impact pressure was estimated at (at least) 600 kPa. The assumption of a flowing avalanche is not supported by the shape of the deposit. Current knowledge of airborne dynamics has a hard time explaining such a high impact pressure.

To conclude it should be noticed that there is currently a limited amount of data on real events. Some of the main parameters, such as the mean density in an airborne avalanche, are still unknown. Thus, many elements of our current knowledge of avalanches have a speculative basis. Today a great deal of work is underway to acquire further reliable data on avalanche dynamics. Experimental

sites, such as *la Sionne* (Switzerland) or the *Lautaret pass* (France), have been developed for that purpose. However a survey of extreme past events shows that the characteristics of extreme avalanches (involving very large volumes) cannot be easily extrapolated from the features of ordinary avalanches. In this respect, the situation is not very different from the problems encountered with large rockfalls and landslides [9,57]. Many observations that hold for ordinary events no longer hold for rare events. Examples include the role of the forest, the influence of the snow type on avalanche motion, etc.

2   Modelling avalanches

Avalanches are extremely complex phenomena. This complexity has led to the development of several approaches based on very different points of view. Many papers and reports have presented an overview of current models. These include the review by Hopfinger [12] as well as a comprehensive up-to-date review of all existing models edited by K. Harbitz [13] in the framework of an European research programme. Here we shall only outline three typical approaches: the statistical approach, the deterministic approach, and small-scale models.

2.1   Statistical methods

In land-use planning (avalanche zoning), the main concern is to delineate areas subject to avalanches. Avalanche mapping generally requires either accurate knowledge of past avalanche extensions or methods for computing avalanche boundaries. To that end several statistical methods have been proposed. The two main models used throughout the world are the one developed by Lied and Bakkehøi [15] and the one developed subsequently by McClung and Lied [14]. Both attempt to predict the extension (stopping position) of the long-return period avalanche for a given avalanche path. Generally, authors have considered avalanches with a return period of approximately 100 year returns. All these methods rely on the correlations existing between the runout distance and some topographic parameters. They assume that the longitudinal profile of the avalanche path governs avalanche dynamics. The topographic parameters generally include the location of the top point of the starting zone (called point A) and a point B of the path profile where the local slope equals a given angle, most often 10° (this point is usually interpreted as the deceleration point of the path). The position of the stopping position (point C) is described using the angle α, which is the angle of the line joining the starting and stopping points with respect to the horizontal (see Fig. 4). Likewise, β is the average inclination of the avalanche path between the horizontal and the line joining the starting point A to point B.

To smooth irregularities in the natural path profile, a regular curve (e.g., a parabola) can be fitted to the longitudinal profile. Statistical methods have so far been applied to flowing avalanches. In principle, nothing precludes using them for airborne avalanches. But in this case, one is faced with the limited amount of
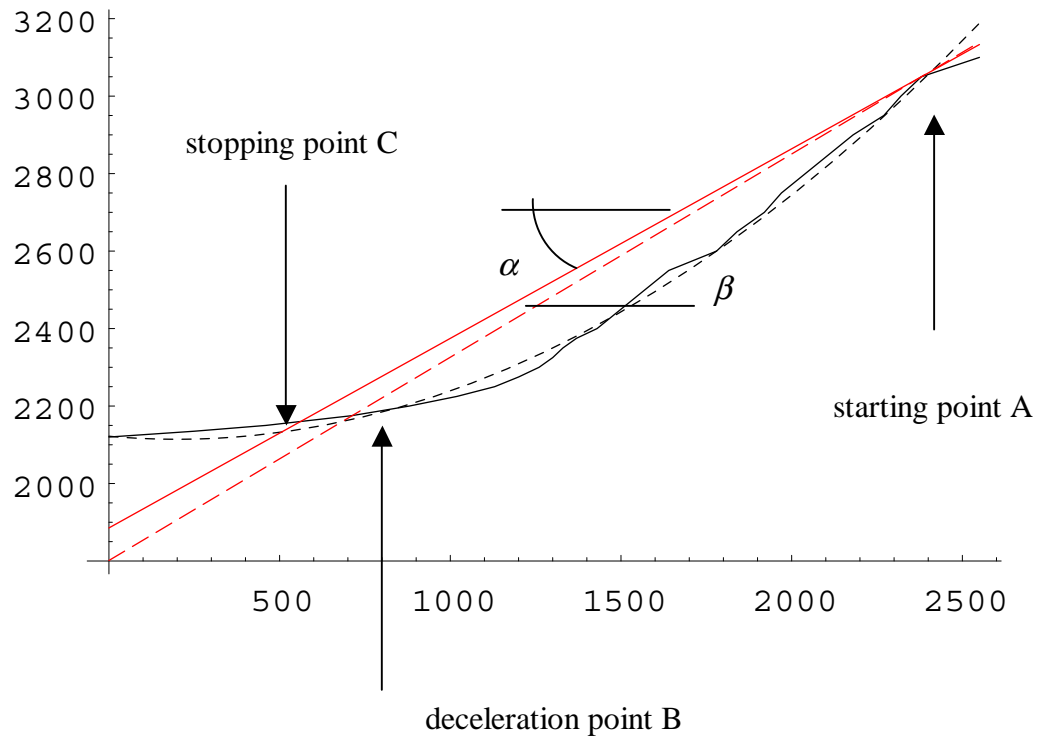
Fig. 4. Topographic parameters describing the profile. The dashed line represents the fitted parabola

data and their poor quality (airborne avalanches are rare and the limits of their deposits are hard to delineate in the field). As an example of statistical models, we indicate the results obtained by Lied and Toppe [16]. Using regression analysis on data corresponding to the longest runout distance observed for 113 avalanche paths in western Norway, these authors have found that:

$$\alpha = 0.96\beta - 1.7°. \tag{1}$$

The regression coefficient is fairly good $(r^2 = 0.93)$ and the standard deviation is relatively small $(s = 1.4°)$. Many extensions of the early model developed by Lied and Bakkehøi have been proposed over the last twenty years either to tune the model parameters to a given mountainous region or adapt the computations to other standards. For instance, subsequent work on statistical prediction of avalanche runout distance has accounted for other topographic parameters such as the inclination of the starting zone or the height difference between the starting and deposition zones. Although statistical methods have been extensively used throughout the world over the last twenty years and have given fairly reliable and objective results, many cases exist in which their estimates are wrong. Such shortcomings can be explained (at least in part) by the fact that for some

avalanche paths, the dynamic behaviour of avalanches cannot be merely related or governed by topographic features.

2.2   Deterministic approach (Avalanche-dynamics models)

The deterministic approach involves quantifying the elementary mechanisms affecting the avalanche motion. Avalanches can be considered at different spatial scales (see Fig. 5). The larger scale, corresponding to the entire flow, leads to the simplest models. The chief parameters include the location of the gravity centre and its velocity. Mechanical behaviour is mainly reflected by the friction force F exerted by the bottom (ground or snowpack) on the avalanche. The smallest scale, close to the size of snow particles involved in the avalanches, leads to complicated rheological and numerical problems. The flow characteristics (velocity, stress) are computed at any point of the occupied space. Intermediate models have also been developed. They benefit from being less complex than three-dimensional numerical models and yet more accurate than simple ones. Such intermediate models are generally obtained by integrating the motion equations across the flow depth in a way similar to what is done in hydraulics for shallow water equations.
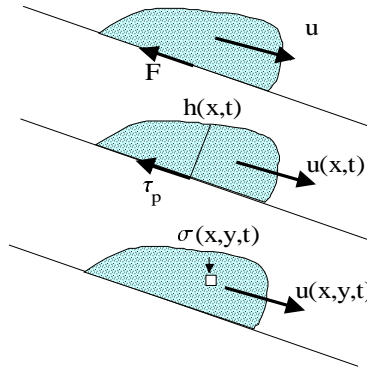

Fig. 5. Different spatial scales used for describing avalanches

Simple models

Simple models have been developed for almost 80 years in order to crude estimations of avalanche features (velocity, pressure, runout distance). They are used extensively in engineering throughout the world. Despite their simplicity and approximate character, they can provide valuable results, the more so as their parameters and the computation procedures combining expert rules and scientific basis have benefited from many improvements over the last few decades.

Simple models for flowing avalanches. The early models date back to the beginning of the 20th century. For the Olympic Games at Chamonix in 1924, the Swiss professor Lagotala computed the velocity of avalanches in the Favrand path [18]. His method was then extended by Voellmy , who popularised it. Since the model proposed by Voellmy (1955), many extensions have been added. The Voellmy-Salm-Gubler (VSG) model [17] and the Perla-Cheng-McClung model [11] are probably the best-known avalanche-dynamics models used throughout the world. Here we outline the VSG model. In this model, a flowing avalanche is considered as a sliding block subject to a friction force:

$$F = mg\frac{u^2}{\xi h} + \mu\, m\, g \cos\theta,$$
(2)

where m denotes the avalanche mass, h its flow depth, θ the local path inclination, μ a friction coefficient related to the snow fluidity, and ξ a coefficient of dynamic friction related to path roughness. If these last two parameters cannot be measured directly, they can be adjusted from several series of past events. It is generally accepted that the friction coefficient μ only depends on the avalanche size and ranges from 0.35 (small avalanches) to 0.155 (very large avalanches) [17]. Likewise, the dynamic parameter ξ reflects the influence of the path on avalanche motion. When an avalanche runs down a wide open rough slope, ξ is close to 400. Conversely, for avalanches moving down confined straight gullies, ξ can be taken as being equal to 1000 or more. In a steady state, the velocity is directly inferred from the momentum balance equation:

$$u = \sqrt{\xi h \cos\theta \left(\tan\theta - \mu\right)}.$$
(3)

According to this equation two flow regimes can occur depending on path inclination. For $\tan\theta > \mu$, (3) has a real solution and a steady regime can occur. For $\tan\theta < \mu$, there is no real solution: the frictional force (2) outweighs the downward component of the gravitational force. It is therefore considered that the flow slows down. The point of the path for which $\tan\theta = \mu$ is called the characteristic point (point P). It plays an important role in avalanche dynamics since it separates flowing and stopping phases. In the stopping zone, we deduce from the momentum equation that the velocity decreases as follows:

$$\frac{1}{2}\frac{du^2}{dx} + u^2\frac{g}{\xi h} = g\cos\theta\left(\tan\theta - \mu\right).$$
(4)

The runout distance is easily inferred from (4) by assuming that at a point $x = 0$, the avalanche velocity is u_p. In practice the origin point is point P but attention must be paid in the fact, according to (3), the velocity at point P should be vanishing; a specific procedure has been developed to avoid this shortcoming (see [17]). Neglecting the slope variations in the stopping zone, we find:

$$x_a = \frac{\xi h}{2g}\ln\left(1 + \frac{u_P^2}{\xi h \cos\theta\left(\mu - \tan\theta\right)}\right).$$
(5)

This kind of model enables us to easily compute the runout distance, the maximum velocities reached by the avalanche on various segments of the path, the flow depth (by assuming that the mass flow rate is constant and given by the initial flow rate just after the release), and the impact pressure.

Simple models for airborne avalanches. For airborne avalanches, simple models have been developed using the analogies with inclined thermals or starting plumes. An inclined thermal consists of the flow of a given volume of a heavy fluid into a surrounding light fluid down an inclined wall. Buoyancy is the key factor of motion. To our knowledge, the earliest model was proposed by Tochon-Danguy and Hopfinger [19], then further developments were made by Béghin and Hopfinger [20], Fukushima and Parker [21], as well as Akiyama and Ura [22]. But as for Voellmy's model, similar models were probably developed in parallel by other authors, notably Russian scientists [23]. The main difficulty encountered here is that avalanche volume increases constantly as the avalanche descends. Thus contrary to simple models developed for flowing avalanches it is necessary to consider a further equation reflecting changes in volume or mass. To that end, it is generally assumed that the avalanche volume is a half ellipsoid (three-dimensional cloud) or a half cylinder with an elliptic basis (two-dimensional cloud). Changes in volume are due to entrainment of surrounding air into the airborne avalanche and snow incorporation from the snow cover. Here, for the sake of simplicity, we only consider two-dimensional flows without snow incorporation. We further assume that the friction exerted by the ground on the cloud is negligible compared to the buoyant force.
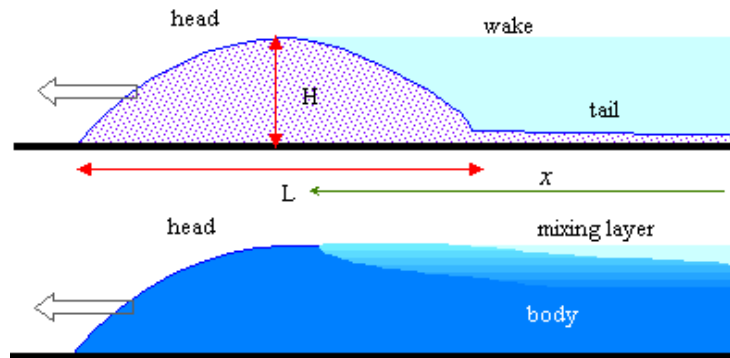

Fig. 6. A thermal is defined as the flow of a constant-volume flow driven by buoyancy (instantaneous release). A starting plume is a constant-supply flow (continuous release).

It is widely recognised (see [25]) that the inflow rate is proportional to a characteristic velocity (generally the mean velocity) and the surface area whatever the type of the flow (jet, plume, thermal) and the environment (uniform or

stratified). Such an assumption leads to:

$$\frac{\mathrm{d}\bar{\varrho}V}{\mathrm{d}t} = \varrho_a \alpha(\theta)SU, \tag{6}$$

where V is the cloud volume, U its velocity (velocity of the mass centre), $\bar{\varrho}$ the mean bulk density of the "heavy" fluid, ϱ_a the density of the ambient ("light") fluid, and the surface area S (per unit width) is $k_s\sqrt{HL}$ with H the flow depth and L the flow length. We can also express the volume V (per unit width) as κHL. We used a shape factor k_s defined by: $k_s = E(1-4k^2)/\sqrt{k}$, where $k = H/L$ and E denotes the elliptic integral function; likewise, κ is another shape factor: $\kappa = \pi/4$. In (6), we have also introduced $\alpha(\theta)$, which is an *entrainment coefficient* depending on the inclination θ only. This assumption needs further explanations. It is usually stated that the entrainment coefficient is a function of an overall *Richardson number*, defined here by: $Ri = g'h\cos\theta/u^2$, where we introduced the reduced gravity $g' = g\Delta\bar{\varrho}/\varrho_a$ and $\Delta\bar{\varrho} = \bar{\varrho} - \varrho_a$ is the buoyant density [24–26]. Here the overall Richardson number reflects the stabilizing effect of the density difference and the relative importance of buoyancy [24]. In the case of a gravity current with constant supply, it is observed that for a given slope, the mean velocity U reaches a constant value, insensitive to slope but depending on the buoyancy flux (per unit width) $A = g'hU$: $U \propto \sqrt[3]{A}$ [24,27]. This also means that the flow adjusts rapidly to a constant Richardson number (for a given slope). In this case, using approximate equations for the mass and momentum balances (respectively $\mathrm{d}(HU)/\mathrm{d}x = \alpha U$ and $\mathrm{d}(HU^2)/\mathrm{d}x = g'h\sin\theta$), we easily deduce that the entrainment coefficient α is a function of the Richardson number and slope: $\alpha = Ri\tan\theta$ [24]. Here, although buoyancy supply is not constant, we assume that the entrainment coefficient α depends only on the slope.

Using the fact that at any time the mean bulk density can be defined by:

$$\bar{\varrho} = \frac{\varrho_0 V_0 + \varrho_a(V - V_0)}{V}, \tag{7}$$

where ϱ_0 and V_0 denote the initial density and volume of the cloud, we infer the volume balance equation:

$$\kappa\frac{\mathrm{d}HL}{\mathrm{d}t} = \alpha(\theta)k_s\sqrt{HL}U. \tag{8}$$

In the present context, Béghin assumed that the ratio $k = H/L$ remains constant from the beginning to the collapse of the cloud. Thus, using the fact that $\mathrm{d}()/\mathrm{d}t = U\mathrm{d}()/\mathrm{d}x$, where the abscissa x refers to the downward position of the mass centre, we easily deduce from (8) that:

$$\frac{\mathrm{d}H}{\mathrm{d}x} = \alpha_H, \tag{9}$$

where $\alpha_H = \alpha(\theta)\sqrt{k}k_s/(2\kappa)$. The ambient fluid exerts two types of pressure on the cloud: a term analogous to a static pressure (Archimede's theorem), equal to $\varrho_a Vg$, and a dynamic pressure. As a first approximation, the latter term can be

evaluated by considering the ambient fluid as an inviscid fluid in a irrotational flow. On the basis of this approximation, it can be shown that the force exerted by the surrounding fluid on the half cylinder is $F_{dyn.} = \varrho_a k_v \mathrm{d}(UV)/\mathrm{d}t$, where $k_v = 2k$ is sometimes called the *added mass coefficient* [28]. Thus the momentum balance equation can be written as:

$$\frac{\mathrm{d}\bar{\varrho}VU}{\mathrm{d}t} = \bar{\varrho}gV \sin\theta - \varrho_a gV \sin\theta - k_v \varrho_a \frac{\mathrm{d}VU}{\mathrm{d}t} \tag{10}$$

or equivalently:

$$\frac{\mathrm{d}(\bar{\varrho} + k_v \varrho_a)VU}{\mathrm{d}t} = \Delta\bar{\varrho}gV \sin\theta. \tag{11}$$

The buoyant term on the right-hand side of (11) is constant. Indeed, using (7), we find that:

$$\Delta\bar{\varrho}gV \sin\theta = \Delta\bar{\varrho}_0 V_0 g \sin\theta \tag{12}$$

with $\Delta\bar{\varrho}_0 = \bar{\varrho}_0 - \varrho_a$ the initial buoyant density. Moreover, to simplify (11), we can use the Boussinesq approximation, which involves neglecting the excess in density in front of the inertial terms ($\bar{\varrho} \approx \varrho_a$). Thus we infer from (11):

$$\frac{\mathrm{d}U^2}{\mathrm{d}x} + \frac{4}{H(x)}\alpha_H U^2 = \frac{2\beta(\theta)}{H^2(x)}, \tag{13}$$

where: $\beta(\theta) = g_0' V_0 \sin\theta / \left(\kappa k(1+k_v)\right)$. After integrating (13), we find that the mean velocity varies as a function of the abscissa as follows:

$$U^2 = \frac{3H_0^4 U_0^2 + 6\beta x H(x) + 2\beta\alpha^2 x^3}{3H^4(x)}, \tag{14}$$

where (U_0, H_0) refer to the initial velocity and depth of the cloud. For large values of x, the mean velocity behaves asymptotically as: $U \propto 1/\sqrt{x}$. The velocity of the front is given by:

$$U_f = \frac{\mathrm{d}}{\mathrm{d}t}(x_f - x + x) = U + \frac{1}{2}\frac{\mathrm{d}}{\mathrm{d}t}L = U\left(1 + \frac{\alpha_H}{2k}\right). \tag{15}$$

Thus the velocity of the front is found to be proportional to the mean velocity. Asymptotically, the front position varies as:

$$U_f \approx \left(1 + \frac{\alpha_H}{2k}\right)\sqrt{\frac{2\beta\alpha^2}{3\alpha_H^4}}\sqrt{\frac{1}{x}} \tag{16}$$

or equivalently:

$$x_f \approx \left(1 + \frac{\alpha_H}{2k}\right)^{2/3}\left(\frac{2}{3}\frac{\alpha^2}{\alpha_H^4}\frac{g_0' V_0 \sin\theta}{\kappa k(1+k_v)}\right)^{1/3} t^{2/3}. \tag{17}$$

This result is of great interest since it is comparable to other results found using different approaches. For instance, using the von Kármán-Benjamin boundary

condition at the leading edge – stating that the front motion is characterized by a constant *Froude number* $Fr = U/\sqrt{gh}$ [i.e., $Fr^2 = g'/(g\,Ri)$] – Huppert and Simpson [29] developed a very simple model, sometimes called the "box model" (see also Chap. ??). They considered a two-dimensional gravity current as a series of equal cross-sectional area rectangles [of length $l(t)$ and height $h(t)$] advancing over a horizontal surface: $u = Fr\sqrt{g'h}$ and $V(t) = h(t)l(t) = V_0$ where V_0 denotes the initial volume (per unit width) of fluid (here $Fr = \sqrt{2}$ inferred from theoretical considerations using the Bernoulli equation [30]). Using $u = \mathrm{d}l/\mathrm{d}t$ and integrating the volume equation leads to:

$$l(t) = \left(\frac{3}{2}Fr\right)^{2/3}(g'V_0)^{1/3}t^{2/3}. \tag{18}$$

Comparison of (17) and (18) reveals the same asymptotic behaviour, except that in Béghin's model, the position depends on the inclination θ. This is both disturbing and comforting since these two models are based on very different approximations: Béghin's model assumes that flow is governed on average by a momentum balance while Huppert and Simpson's model states that the flow behaviour is dictated by dynamic conditions at the leading edge. Many experiments have been performed on the motion of a two-dimensional cloud over horizontal surfaces or down inclined planes (Britter [31,27], Simpson [33], Huppert [29], Rottman [32], Béghin [20,34], Fukushima [35], Hallworth [36], Bonnecaze [38,37], Hatcher [39], etc.). They have confirmed the theoretical trend displayed in (16) or (17). The main difference between experimental results concerns the depth increase rate α_H (ranging from 0.01 to 0.02 for $\theta = 5°$).

Many field and laboratory observations have shown the significant role played by particle sedimentation or incorporation of material from the ground into the cloud. Improvements of existing simple models have been achieved by implementing new procedures taking material entrainment into account. Research on this topic is still in process. Compared to field data, Béghin's model usually provides correct estimates of the mean front velocity (to 20%) but it may substantially underestimate the impact pressure by a factor 10. The reason why the impact pressure computed as $\varrho u^2/2$ is underestimated is not clear. Very large velocity fluctuations inside the airborne avalanche or particles clustering at the flow bottom may be responsible for very high impact pressures. Another field observation that cannot be explained by Béghin-type models is the considerable acceleration at the early stages of an aerosol; in some cases, acceleration of $6\,\mathrm{m/s}^2$ over a $40°$ slope has been recorded for more than $5\,\mathrm{s}$. This may also be related to the controversy on reduced gravity [40]. Indeed, some authors have claimed that a flow acceleration scaling as g' is not physical and suggested the alternative g'' defined by $g'' = g(\bar{\varrho} - \varrho_a)/\bar{\varrho}$. Concerning avalanches, field data tend to show that avalanche acceleration scales as g'.

Intermediate models (depth-averaged models)

Simple models can provide approximate predictions concerning runout distance, the impact pressure, or deposit thickness. However they are limited for many

reasons. For instance, they are restricted to one-dimensional path profiles (the spreading of the avalanche cannot be computed) and the parameters used are fitted to past events and cannot be measured in the field or in the laboratory (rheometry), apart from airborne models if the analogy with turbidity currents is used. More refined models use depth-averaged mass and momentum equations to compute the flow characteristics. With such models, the limitations of simple models are alleviated. For instance it is possible to compute the spreading of avalanches in their runout zone or relate mechanical parameters used in the models to the rheological properties of snow. As far as we know, the early depth-averaged models were developed in the 1970s by Russian scientists (Kulikovskii, Eglit [23,41,42]) and French researchers (Pochat, Brugnot, Vila [43,44]) for flowing avalanches. For airborne avalanches, the first stage was probably the model developed by Parker, Fukushima, and Pantin [45], which, though devoted to submarine turbidity currents, contains almost all the ingredients used in subsequent models of airborne avalanches. Considerable progress in the development of numerical depth-averaged models has been made possible thanks to the increase in computer power and breakthrough in the numerical treatment of hyperbolic partial differential equation systems (see [46] for a comprehensive review on hyperbolic differential equations in physics and [47] for a practical introduction to numerical treatment).

Depth-averaged motion equations. Here, we shall address the issue of slightly transient flows. We focus exclusively on *gradually varied flows*, namely flows that are not far from a steady uniform state for the time interval under consideration. Moreover, we first consider flows without entrainment of the surrounding fluid and variation in density: $\varrho \approx \bar{\varrho}$. Accordingly the bulk density may be merely replaced by its mean value. In this context, the motion equations may be inferred in a way similar to the usual procedure used in hydraulics to derive the shallow water equations (or Saint-Venant equations): it involves integrating the momentum and mass balance equations over the depth. As such a method has been extensively used in hydraulics for water flow [50] as well for non-Newtonian fluids (see for instance Parker, Fukushima, and Pantin [45], Savage and Hutter [48] or Piau [49]; see also Chap. **??**) we shall briefly recall the principle and then directly provide the resulting motion equations. Let us consider the local mass balance: $\partial \varrho/\partial t + \nabla.(\varrho \mathbf{u}) = 0$. Integrating this equation over the flow depth leads to:

$$\int\limits_{0}^{h(x,t)} \left(\frac{\partial u}{\partial x} + \frac{\partial v}{\partial y} \right) \mathrm{d}y = \frac{\partial}{\partial x} \int\limits_{0}^{h} u(x,y,t)\mathrm{d}y - u(h)\frac{\partial h}{\partial x} - v(x,h,t) - v(x,0,t), \quad (19)$$

where u and v denote the x- and y-component of the local velocity. At the free surface and the bottom, the y-component of velocity satisfies the following boundary conditions:

$$v(x,h,t) = \frac{dh}{dt} = \frac{\partial h}{\partial t} + u(x,h,t)\frac{\partial h}{\partial x}, \quad (20)$$

$$v(x, 0, t) = 0. \tag{21}$$

We easily deduce:

$$\frac{\partial h}{\partial t} + \frac{\partial h\overline{u}}{\partial x} = 0. \tag{22}$$

where we have introduced depth-averaged values defined as:

$$\bar{f}(x, t) = \frac{1}{h(x, t)} \int_0^{h(x,t)} f(x, y, t) \mathrm{d}y. \tag{23}$$

The same procedure is applied to the momentum balance equation: $\mathrm{d}\boldsymbol{u}/\mathrm{d}t = \rho\boldsymbol{g} + \nabla.\boldsymbol{\sigma}$, where $\boldsymbol{\sigma}$ denotes the stress tensor. Without difficulty, we can deduce the averaged momentum equation from the x-component of the momentum equation:

$$\bar{\varrho}\left(\frac{\partial h\overline{u}}{\partial t} + \frac{\partial h\overline{u^2}}{\partial x}\right) = \bar{\varrho}gh\sin\theta + \frac{\partial h\bar{\sigma}_{xx}}{\partial x} - \tau_p, \tag{24}$$

where we have introduced the bottom shear stress: $\tau_p = \sigma_{xy}(x, 0, t)$. In the present form, the motion equation system (24 and 22) is not closed since the number of variables exceeds the number of equations. A common approximation involves introducing a parameter (sometimes called the Boussinesq momentum coefficient) which links the mean velocity to the mean square velocity:

$$\overline{u^2} = \frac{1}{h} \int_0^h u^2(y)\, dy = \alpha\bar{u}^2. \tag{25}$$

Another helpful (and common) approximation, not mentioned in the above system, concerns the computation of stress [50]. Putting ourselves in the framework of long wave approximation, we assume that longitudinal motion outweighs vertical motion: for any quantity m related to motion, we have $\partial m/\partial y \gg \partial m/\partial x$. This allows us to consider that every vertical slice of flow can be treated as if it was locally uniform. In such conditions, it is possible to infer the bottom shear stress by extrapolating its steady-state value and expressing it as a function of u and h. A point often neglected is that this method and its results are only valid for flow regimes that are not too far away from a steady-state uniform regime. In flow parts where there are significant variations in the flow depth (e.g. at the leading edge and when the flow widens or narrows substantially), corrections should be made to the first-order approximation of stress [49]. Finally, an unresolved problem concerns the nature of the front in a transient flow. The same problem has been already pointed out above in the discussion on Béghin's model and "box models". Some authors have considered it as a shock; in this case, it is included in the motion equations as a downstream boundary condition [42–44]. In contrast, authors have implicitly assumed that the front has no specific dynamic role and can be generated by the hyperbolic motion equations [51]. Other authors considered that the front may be controlled by gravity unstability. For

instance, numerous experiments performed on viscous and buoyant gravity currents have revealed that a shifting pattern of lobes and clefts ranges across the front due to a gravity instability [52–54].

Flowing avalanches. The material is very concentrated in ice particles: generally the concentration ranges from 20% to 65%. The material is highly compressible (it is frequent to observe snow densities in the deposition zone three times larger than in the starting zone). This is due to the intrinsic compressibity of snow as well as dilatant behaviour when the material contains snow balls. The rheology of ice/air mixtures is rather complex: significant variations in the mixture composition are caused by minute changes in the air temperature around $0°$ C. This explains the considerable variability of snow consistency: granular (snow ball), loose, slush-like or pasty snow. The diversity of snow consistency, along with the size scales, makes any thorough rheometrical examination of snow involved in avalanches a tricky undertaking. To date, few experimental studies have been devoted to this topic. The authors (such as Dent [55] or Maeno and Nishimura [56]), who studied the rheological bulk behaviour of snow, have generally found that snow is a non-Newtonian viscoplastic material, which depends a great deal on density. Several constitutive equations have been proposed: Newtonian fluid, Reiner-Ericken fluid, Bingham fluid, frictional Coulombic fluid, and so on. For instance, Savage and Hutter assumed that flowing avalanches have many similarities with dry granular flows [10,48]. They have further assumed that, as a first approximation, the Coulomb law can be used to describe the bulk behaviour of flowing granular materials. Therefore they have expressed the bottom shear stress as: $\tau_p = \varrho g h \tan \delta \cos \theta$, where δ denotes a bed friction angle. Likewise, the normal mean shear stress can be written as: $\bar{\sigma}_{xx} = -k_a \varrho g h \cos \theta / 2$, where the coefficient k_a is related to the earth pressure coefficient used in soil mechanics. Eventually they obtained for flows down inclined planes:

$$\frac{\partial h}{\partial t} + \frac{\partial h \overline{u}}{\partial x} = 0, \tag{26}$$

$$\frac{\partial \bar{u}}{\partial t} + \bar{u} \frac{\partial \bar{u}}{\partial x} = g \cos \theta \left(\tan \theta - \tan \delta \right) - k_a g \cos \theta \frac{\partial h}{\partial x}. \tag{27}$$

Laboratory tests with dry granular media have shown that such a model captures the flow features well for steep smooth inclined channels [10,57–59]. Similar models were developed using different constitutive equations. For instance, Eglit used empirical expressions for the bottom shear stress (in a form similar to (2)) and treated the leading edge using a specific boundary condition [42,41]. Naaim and Ancey used a Bingham constitutive equation in their model [60]. All these models must deal with the difficult problem of fitting rheological parameters. Due to the lack of relevant rheological data on snow, the parameters are usually adjusted for the runout distance to coincide with field data.

Airborne avalanches. An airborne avalanche is a very turbulent flow of a dilute ice-particle suspension in air. It can be considered as a one-phase flow

as a first approximation. Indeed, the Stokes number defined as the ratio of a characteristic time of the fluid to the relaxation time of the particles is low, implying that particles adjust quickly to changes in the air motion [61]. At the particle scale, fluid turbulence is high enough to strongly shake the mixture since the particle size is quite small. To take into account particle sedimentation, authors generally consider airborne avalanches as turbulent stratified flows. Thus, contrary to flowing avalanches, bulk behaviour is well identified in the case of airborne avalanches. The main differences between the various models proposed result from the different boundary conditions, use of the Boussinesq approximation, and the closure equations for turbulence. Parker and his co-workers [45] developed a complete depth-averaged model for turbidity currents. The motion equation set proposed by these authors is more complicated than the corresponding set for dense flows presented above, since it includes additional equations arising from the mass balance for the dispersed phase, the mean and turbulent kinetic energy balances, and the boundary conditions related to the entrainment of sediment and surrounding fluid:

$$\frac{\partial h}{\partial t} + \frac{\partial hU}{\partial x} = E_a U, \tag{28}$$

$$\frac{\partial (Ch)}{\partial t} + \frac{\partial (hUC)}{\partial x} = v_s E_s - v_s c_b, \tag{29}$$

$$\frac{\partial hU}{\partial t} + \frac{\partial hU^2}{\partial x} = RCgh\sin\theta - \frac{1}{2}Rg\frac{\partial Ch^2}{\partial x} - u_*^2, \tag{30}$$

$$\frac{\partial hK}{\partial t} + \frac{\partial hUK}{\partial x} = \frac{1}{2}E_a U^3 + u_*^2 U - \varepsilon_0 h - \frac{1}{2}E_a U RCgh - RCghv_s - \frac{1}{2}Rghv_s\left(E_s - c_b\right), \tag{31}$$

where U is the mean velocity, h the flow depth, K the mean turbulent kinetic energy, C the mean volume concentration (ratio of particle volume to total volume), E_a a coefficient of entrainment of surrounding fluid into the current, v_s the settlement velocity, E_s a coefficient of entrainment of particles from the bed into the current, c_b the near-bed particle concentration, R the specific submerged gravity of particles (ratio of buoyant density to ambient fluid density), u_*^2 the bed shear velocity, and ε_0 the depth-averaged mean rate of dissipation of turbulent energy due to viscosity. The main physical assumption in Parker *et al.*'s model is that the flow is considered as one-phase from a momentum point of view but treated as two-phase concerning the mass balance. Equation (28) states that the total volume variation results from entrainment of surrounding fluid. In (29), the variation in the mean solid concentration is due to the difference between the rate of particles entrained from the bed and the sedimentation rate. Equation (30) is the momentum balance equation: the momentum variation results from the driving action of gravity and the resisting action of bottom shear stress; depending on the flow depth profile, the pressure gradient can contribute either

to accelerate or decelerate the flow. Equation (31) takes into account the turbulence expenditure for the particles to stay in suspension. Turbulent energy is supplied by the boundary layers (at the flow interfaces with the surrounding fluid and the bottom). Turbulent energy is lost by viscous dissipation ($\varepsilon_0 h$ in (31)) as well as by mixing the flow (fourth and fifth terms in (31)) and maintaining the suspension against sedimentation flow mixing (last term on the right-hand side of (31)). Although originally devoted to submarine turbidity currents, this model has been applied to airborne avalanches, with only small modifications in the entrainment functions (Fukushima and Parker [21], Gauer [62]). Further developments have been brought to the primary model proposed by Parker *et al.*, notably in order to consider non-Boussinesq fluids and snow entrainment from the snowcover [63]. To our knowledge, such models do not currently provide better results than simple models when compared to field data.

Three-dimensional computational models.

The rapid increase in computer power has allowed researchers to integrate local motion equations directly. Compared to the depth-averaged models, the problems in the development of three-dimensional (3D) computational models mainly concern numerical treatments. For instance, the treatment of the free surface poses complicated issues. Naturally, problems linked to the constitutive equations reliable for snow are more pronounced compared to intermediate models since the entire constitutive equation must be known (not just the shear and normal stress). The development of 3D models is currently undertaken mainly for airborne avalanches generally using finite-volume codes for turbulent flows. Examples include the models by Naaim [64], Hermann [66], Schweiwiller and Hutter [65], etc.

2.3   Small-scale models

A few authors have exploited the similarities between avalanches and other gravity-driven flows. For instance, Hopfinger and Tochon-Danguy used the analogy between airborne avalanches and saline density currents to perform experiments in the laboratory in a water tank [67]. In this way, examination of various aspects of airborne dynamics has been possible: effect of a dam, structure of the cloud, determination of the entrainment coefficients, etc. The chief issue raised by the analogy with density or gravity currents concerns the similarity conditions based on both the Froude (or equally the Richardson number) and Reynolds numbers [12,34,67]. Regarding flowing avalanches, authors have considered the analogy with granular flows. Various materials (ping pong ball, sand, beads) have been used. In engineering laboratory experiments simulating flowing avalanches offer promising tools for studying practical and complicated issues, such as the deflecting action of a dam [68] or braking mounds [69]. A few scientists have conducted or are performing experiments studying snow flows down confined geometries the field [70].

References

1. A. Roch: *Neve e Valanghe* (Club Alpino Italiano, Torino, 1980)
2. C. Ancey: *Guide Neige et Avalanches : Connaissances, Pratiques, Sécurité*, 2nd edn. (Edisud, Aix-en-Provence, 1998)
3. W. Amman, O. Buser, U. Vollenwyder: *Lawinen* (Birhäuser, Basel, 1997)
4. D. M. McClung, P. A. Schaerer: *The avalanche handbook* (The Montaineers, Seattle, 1993)
5. T. Daffern: *Avalanche Safety for Skiers & Climbers* (Rocky Mountain Books, Calgary, 1992)
6. W. Munter: *Lawinen, entscheiden in kritischen Situationen* (Agentur Pohl und Schellhammer, Garmisch Partenkirchen, 1997)
7. R. de Quervain: *Avalanche Atlas* (Unesco, Paris, 1981)
8. A. I. Mears: *Snow-avalanche hazard analysis for land-use planning and Engineering*. Bulletin **49** (Colorado Geological Survey, Denver, 1992)
9. K. J. Hsü: 'Albert Heim: observations on landslides and relevance to modern interpretations'. In: *Rockslides and avalanches* ed. By B. Voight (Elsevier, Amsterdam, 1978) pp. 71-93
10. S. B. Savage: 'Flow of granular materials'. In: *Theoretical and Applied Mechanics* ed. by P. Germain, J.-M. Piau, D. Caillerie (Elsevier, Amsterdam, 1989) pp. 241-266
11. R. Perla, T. T. Cheng, D. M. Mc Clung: J. Glaciol. **26**, 197 (1980)
12. E. J. Hopfinger: Annu. Rev. Fluid Mech. **15**, 45 (1983)
13. K. Harbitz: 'A survey of computational models for snow avalanche motion'. In: *final report of Avalanche Mapping, Model Validation and Warning Systems*, (Fourth European Framework Programme, ENV4- CT96-0258, Brussels, 1999)
14. D. M. McClung, K. Lied: Cold Reg. Sci. Technol. **13**, 107 (1987)
15. K. Lied, S. Bakkehøi: J. Glaciol. **26**, 165 (1980)
16. K. Lied, R. Toppe: Ann. Glaciol. **13**, 164 (1989)
17. B. Salm, A. Burkard, H. Gubler: *Berechnung von Fliesslawinen, eine Anleitung für Praktiker mit Beispielen*. Report **47** (EISFL, Davos, 1990)
18. H. Lagotala: *Etude de l'avalanche des Pélerins (Chamonix)*, (Société Générale d'Imprimerie, Genève, 1927)
19. J.-C. Tochon-Danguy, E. J. Hopfinger: 'Simulation of the dynamics of powder avalanches'. In: *International symposium on snow mechanics, Grindelwald, 1974*, IAHS Publication 144 (IAHS, 1974) pp. 369-380
20. P. Beghin, E. J. Hopfinger, R. E. Britter: J. Fluid Mech. **107**, 407 (1981)
21. Y. Fukushima, G. Parker: J. Glaciol. **36**, 229 (1990)
22. J. Akiyama, M. Ura: J. Hydraul. Eng. ASCE **125**, 474 (1999)
23. N. Bozhinskiy, K. S. Losev: *The fundamentals of avalanche science*. Report **55** (EISLF, Davos, 1998)
24. J. S. Turner: *Buoyancy effects in fluids* (Cambridge University Press, Cambridge, 1973)
25. J. S. Turner: J. Fluid Mech. **173**, 431 (1986)
26. G. Parker, M. Garcia, Y. Fukushima, W. Yu: J. Hydr. Res. **25**, 123 (1987)
27. R. E. Britter, P. F. Linden: J. Fluid Mech. **99**, 531 (1980)
28. G. K. Batchelor: *An introduction to fluid dynamics* (Cambridge University Press, 1967)
29. H. E. Huppert, J. E. Simpson: J. Fluid Mech. **99**, 785 (1980)
30. T. B. Benjamin: J. Fluid Mech. **31**, 209 (1968)
31. R. E. Britter, J. E. Simpson: J. Fluid Mech. **88**, 223 (1978)

32. J. W. Rottman, J. E. Simpson: J. Fluid Mech. **135**, 95 (1983)
33. J. E. Simpson, R. E. Britter: J. Fluid Mech. **94**, 477 (1979)
34. P. Beghin, X. Olagne: Cold Reg. Sci. Technol. **19**, 317 (1991)
35. Y. Fukushima, N. Hayakawa: J. Hydraul. Eng. ASCE **121**, 600 (1995)
36. M. A. Hallworth, A. Hogg, H. E. Huppert: J. Fluid Mech. **359**, 109 (1998)
37. R. T. Bonnecaze, M. A. Hallworth, H. E. Huppert, J. R. Lister: J. Fluid Mech. **294**, 93 (1995)
38. R. T. Bonnecaze, H. E. Huppert, J. R. Lister: J. Fluid Mech. **250**, 339 (1993)
39. L. Hatcher, A. Hogg, A. W. Woods: J. Fluid Mech. **416**, 297 (2000)
40. H. P. Gröbelbauer, T. K. Fanneløp, R. E. Britter: J. Fluid Mech. **250**, 669 (1993)
41. M. Eglit: 'Mathematical modeling of dense avalanches'. In: *25 years of snow avalanche research, Voss, 1998* ed. by E. Hestnes (Norwegian Geotechnical Institute, 1998) pp. 15-18
42. E. M. Eglit: 'Some mathematical models of snow avalanches'. In: *Advances in the mechanics and the flow of granular materials* ed. by M. Shahinpoor (Trans Tech Publications, 1983 of Conference) pp. 577-588
43. G. Brugnot, R. Pochat: J. Glaciol. **27**, 77 (1981)
44. J. P. Vila: Sur la théorie et l'approximation numérique des problèmes hyperboliques non linéaires, application aux équations de Saint-Venant et à la modélisation des avalanches denses. Ph.D. Thesis, University Paris VI, (1986)
45. G. Parker, Y. Fukushima, H. M. Pantin: J. Fluid Mech. **171**, 145 (1986)
46. G. B. Whitham: *Linear and nonlinear waves*, 2nd edn. (John Wiley & Sons, New York, 1999)
47. E. F. Toro: *Riemann solvers and numerical methods for fluid dynamics* (Springer, Berlin, 1997)
48. S. B. Savage, K. Hutter: Acta Mech. **86**, 201 (1991)
49. J.-M. Piau: J. Rheol. **40**, 711 (1996)
50. V. T. Chow: *Open-channel Hydraulics* (Mc Graw Hill, New York, 1959)
51. M. Wieland, J. M. N. T. Gray, K. Hutter: J. Fluid Mech. **392**, 73 (1999)
52. J. E. Simpson: J. Fluid Mech. **53**, 759 (1972)
53. C. Härtel, E. Meiburg, F. Necker: J. Fluid Mech. **418**, 189 (2000); *ibid* 213
54. D. Snyder, S. Tait: J. Fluid Mech. **369**, 1 (1998)
55. J. D. Dent, T. E. Lang: Ann. Glaciol. **4**, 42 (1983)
56. O. Maeno: 'Rheological characteristics of snow flows'. In: *International Workshop on Gravitational Mass Movements, Grenoble, 1993* ed. by L. Buisson (Cemagref, 1993) pp. 209-220
57. S. B. Savage, K. Hutter: J. Fluid Mech. **199**, 177 (1989)
58. K. Hutter, T. Koch, C. Plss, S. B. Savage: Acta Mech. **109**, 127 (1995)
59. K. Hutter, M. Siegel, S. B. Savage, Y. Nohguchi: Acta Mech. **100**, 37 (1993)
60. C. Ancey, M. Naaim: 'Modelisation of dense avalanches'. In: *Université européenne d'été sur les risques naturels, Chamonix, 1992* ed. by G. Brugnot (Cemagref, Antony, 1995) pp. 173-182
61. G. K. Batchelor: 'A brief guide to two-phase flow'. In: *Theoretical and Applied Mechanics* ed. by P. Germain, J. M. Piau, D. Caillerie (Elsevier, Amsterdam, 1989) pp 27-41
62. P. Gauer: 'A model of powder snow avalanche'. In: *Les apports de la recherche scientifique à la sécurité neige, glace et avalanche, Chamonix, 1995* ed. by F. Sivardière (Cemagref, 1995), pp. 55-61
63. D. Issler: Ann. Glaciol. **26**, 253 (1998)
64. M. Naaim, I. Gurer: J. Natural Hazard **16**, 18 (1997)

65. T. Scheiwiller, K. Hutter, F. Hermann: Ann. Geophys. **5B**, 569 (1987)
66. F. Hermann, D. Issler, S. Keller: 'Numerical simulations of powder-snow avalanches and laboratory experiments in turbidity currents'. In: *International Workshop on Gravitational Mass Movements, Grenoble, 1993* ed. by L. Buisson (Cemagref, 1993) pp. 137-144
67. E. J. Hopfinger, J.-C. Tochon-Danguy: J. Glaciol. **81**, 343 (1977)
68. T. Chu: Can. Geotech. J. **32**, 285 (1995)
69. K. M. Hàkonardóttir: Retarding effects of breaking mounds-avalanches. MA dissertation, University of Bristol, Bristol (2000)
70. J. D. Dent, K. J. Burrell, D. S. Schmidt, M. Y. Louge, E. E. Adams, T. G. Jazbutis: Ann. Glaciol. **26**, 243 (1998)